Chinese Chemical Letters 32 (2021) 3215–3220

Contents lists available at ScienceDirect

Chinese Chemical Letters

journal homepage: www.elsevier.com/locate/cclet

Communication

Photocatalytic degradation of sulfadiazine in suspensions of TiO_2 nanosheets with exposed (001) facets

Xiaofan Xiang[a,1], Laiyan Wu[a,*,1], Junjiang Zhu[b], Jiazhou Li[a], Xi Liao[a], Hongcheng Huang[a], Jiajie Fan[c], Kangle Lv[a,*]

[a] Key Laboratory of Resources Conversion and Pollution Control of the State Ethnic Affairs Commission, College of Resources and Environmental Science, South-Central University for Nationalities, Wuhan 430074, China
[b] Hubei Key Laboratory of Biomass Fibers and Eco-Dyeing & Finishing, College of Chemistry and Chemical Engineering, Wuhan Textile University, Wuhan 430200, China
[c] School of Materials Science and Engineering, Zhengzhou University, Zhengzhou 450001, China

ARTICLE INFO

Article history:
Received 6 December 2020
Received in revised form 24 January 2021
Accepted 24 March 2021
Available online 26 March 2021

Keywords:
Sulfadiazine
Antibiotics
Photocatalytic degradation
TiO_2 nanosheets
Degradation pathway

ABSTRACT

Antibiotics such as sulfonamides are widely used in agriculture as growth promoters and medicine in treatment of infectious diseases. However, the release of these antibiotics has caused serious environmental problems. In this paper, photocatalytic oxidation technology was used to degrade sulfadiazine (SDZ), one of the typical sulfonamides antibiotics, in UV illuminated TiO_2 suspensions. It was found that TiO_2 nanosheets (TiO_2-NSs) with exposed (001) facets exhibit much higher photoreactivity towards SDZ degradation compared to TiO_2 nanoparticles (TiO_2-NPs) with a rate constant increases from 0.017 min^{-1} to 0.035 min^{-1}, improving by a factor of 2.1. Under the attacking of reactive oxygen species (ROSs) such as superoxide radicals ($^{\bullet}O_2^-$) and hydroxyl radicals ($^{\bullet}OH$), SDZ was steady degraded on the surface of TiO_2-NSs. Based on the identification of the produced intermediates by LC–MS/MS, possible degradation pathways of SDZ, which include desulfonation, oxidation and cleavage, were put forwards. After UV irradiation for 4 h, nearly 90% of the total organic carbon (TOC) can be removed in suspensions of TiO_2-NSs, indicating the mineralization of SDZ. TiO_2-NSs also exhibits excellent stability in photocatalytic degradation of SDZ in wide range of pH. Even after recycling used for 7 times, more than 91.3% of the SDZ can be efficiently removed, indicating that they are promising to be practically used in treatment of wastewater containing antibiotics.

Sulfonamides (SNs) antibiotics are widely used in agriculture as growth promoters and medicine in treating of infectious diseases due to their low cost and high efficiency [1,2]. However, the release of unconsumed antibiotics will spread widely and cause serious environmental problems. For example, sulfadiazine (SDZ), one type of sulfonamides antibiotics, has been widely detected in various environmental compartments such as WWTPs, hospitals and river water [3–6]. In China, about 1260 tons of SDZ was used each year, which is the second largest used antibiotic in the common sulfonamides family [7]. The uncontrolled use of SDZ and its exposure to environment would lead to potential health risk and ecological impacts, and therefore received increasing concerns in the past decades [8].

Although a lot of attention has been drawn on the removal of SDZ in aquatic environment, traditional methods such as adsorption, biodegradation, chlorination and ozonation are ineffective for SDZ removal because of the microbial inhibition and disinfection byproducts (DBPs) formation [9–11]. Therefore, new techniques to effectively decompose SDZ in wastewater are urgently anticipated but remain a great challenge.

Recently, great attentions have been paid to advanced oxidation technologies (AOTs) [12–15], especially semiconductor photocatalysis, as they provide a sustainable way to solve the environmental problems [16–19]. Upon irradiation, the photo-generated carriers (electrons and holes) will migrate to the surface of the photocatalyst. The electrons will be captured by surface adsorbed oxygen to produce superoxide radicals ($^{\bullet}O_2^-$), while hole will oxidize the surface adsorbed H_2O to produce the produced hydroxyl radicals ($^{\bullet}OH$). These reactive oxygen species (ROSs) are strong oxidants, which can attack the organics in solution, resulting in the

* Corresponding authors.
E-mail addresses: wulaiyan@mail.scuec.edu.cn (L. Wu), lvkangle@mail.scuec.edu.cn, lvkangle888@163.com (K. Lv).
[1] These authors contributed equally to this work.

https://doi.org/10.1016/j.cclet.2021.03.064
1001-8417/

decomposition and even mineralization of organic pollutants [20,21].

Among all the semiconductor photocatalysts, TiO_2 is the most popular due to its strong oxidation power, chemical inertness and excellent biocompatibility [22–25]. However, the quantum efficiency of TiO_2 photocatalysis is not high enough due to the quick recombination of charge carriers [26]. To overcome the limitations of bare TiO_2, researches have focused on the modification of TiO_2-based materials by introduction of surface oxygen vacancy [27], doping with heteroatoms [28,29] and coupling with another semiconductor photocatalyst to form heterojunctions [30,31]. In 2008, Yang *et al.* successfully fabricated high energy TiO_2 nanocrystals with exposed (001) facets using HF as shape-directing agent [32]. As (001) facet of anatase TiO_2 is more reactive than (101) facet, the study of high energy TiO_2 becomes a hot topic [33]. Our previous study showed that the high photoreactivity of high energy TiO_2 nanocrystal is ascribed to the combination of exposed reactive (001) facets and surface fluorination [34,35]. According to the study of Murakami *et al.*, TiO_2 nanocrystals with exposed high energy facets can drive electrons and holes to different crystal faces. The spatial separation of photo-generated electrons and holes can efficiently retard the recombination, enhancing the photocatalytic activity [36].

On considering the high photoreactivity of high energy faceted TiO_2, anatase TiO_2 nanosheets (TiO_2-NSs) exposed predominant high-energy (001) facets was prepared, which was used for photocatalytic degradation of SDZ. The degradation pathway of SDZ over the TiO_2-NSs was also investigated based on the determination of the produced intermediates by LC–MS/MS techniques.

XRD was used to identify the phase structures of the semiconductor photocatalysts, and the results are shown in Fig. 1A. It can be seen that both TiO_2-NPs and TiO_2-NSs are pure anatase TiO_2 with the XRD diffraction peaks at around $2\theta = 25.3^\circ$, 37.9° and 48.1°, corresponding to the (101), (004) and (200) plane diffraction of anatase TiO_2 (JCPDS No. 21-1272) [37]. Careful view shows that the (004) peak intensity of TiO_2-NSs is weaker, while the intensity of the (200) peak is much stronger than that of TiO_2-NPs. According to Scherrer equation, the crystalline sizes of anatase TiO_2-NSs along (001) and (100) directions are 6.0 nm and 30.9 nm, respectively. As for TiO_2-NPs, the crystalline sizes along (001) and (100) directions are 11.3 nm and 9.1 nm, respectively. These results suggest that the presence of shape-controlling agent (HF) results in the preferential growth of TiO_2 nanocrystals along a-axis, resulting in the exposure of high-energy (001) facets.

According to the study of Yang *et al.*, the average surface energy for (001) facets (0.90 J/m^2) is much higher than that of (101) facets (0.44 J/m^2). Then anatase TiO_2 crystals usually exhibit octahedral bipyramidal shape with exposed 8 thermodynamically stable (101) facets. However, the strong adsorption of fluoride ions on the surface of TiO_2 nanocrystals can reverse the surface energy of (001) and (101) facets, resulting in the exposure of more reactive (001) facets [32].

Fig. 1B compares the diffuse reflectance spectra of the photocatalysts in UV and visible regions. It can be seen that TiO_2-NPs exhibits slightly higher light-harvesting ability than TiO_2-NSs in UV region, although both samples have the same light-absorption edge of 390 nm, corresponding to a bandgap of 3.18 eV.

The bipyramidal shaped TiO_2-NPs can be observed from the TEM image (Fig. S1A in Supporting information). Fig. S1B (Supporting information) is the high resolution TEM (HRTEM) image of TiO_2-NPs, from which we can see a truncated octahedral bipyramidal shaped TiO_2 nanocrystal with width of *ca.* 14 nm (along the a-axis) and thickness of *ca.* 20 nm (along the c-axis).

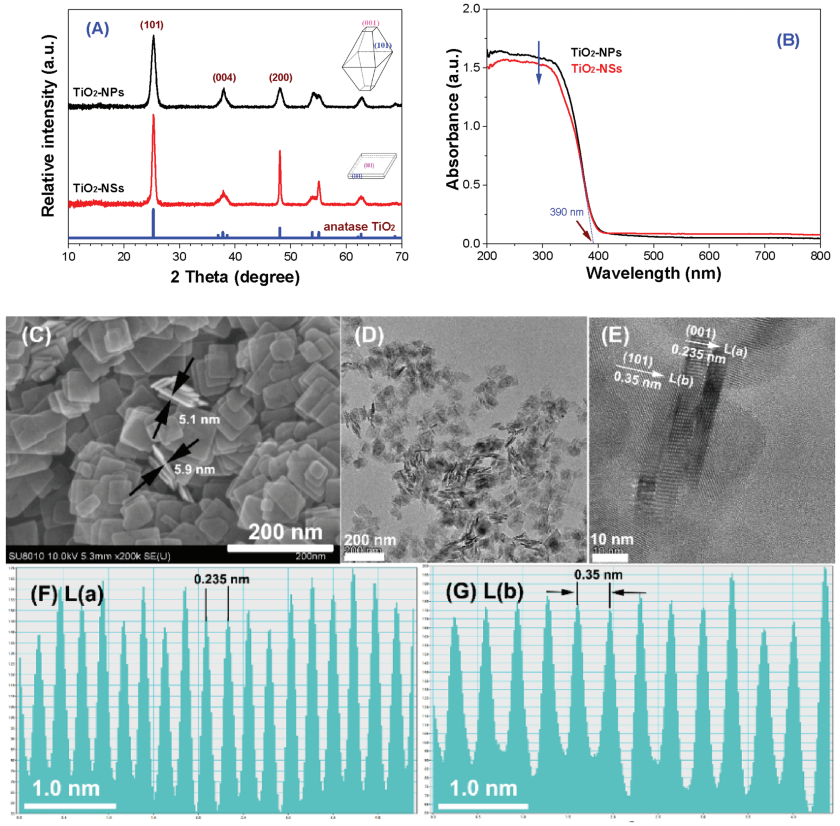

Fig. 1. Comparison of the XRD patterns (A) and diffuse reflectance spectra (B) of the photocatalysts, SEM (C) and TEM (D and E) images of TiO_2-NSs. (F) and (G) are the corresponding intensity profiles from the high resolution TEM image of TiO_2-NSs (E) along line (a) and line (b), respectively.

On the contrary, in the presence of shape-directing agent, sheet-like TiO_2 nanocrystals with sidelength of 40–50 nm and thickness of about 5–6 nm were obtained (Figs. 1C and D). The HR TEM image of TiO_2-NSs is shown in Fig. 1E. From the side view of the HR TEM image, we can see that the lattice spacing parallel to the top and bottom facets is *ca.* 0.235 nm (see intensity profile in Fig. 1F), which is corresponding to the (001) planes of anatase TiO_2. While the TiO_2 nanosheets lying on the grid have a rectangular outline with a lattice spacing of *ca.* 0.35 nm, which is corresponding to the (101) planes of anatase TiO_2 (see intensity profile in Fig. 1G).

SDZ is very stable, which exhibits little degradation in the absence of any photocatalyst even under the UV irradiation. However, in the presence of TiO_2 photocatalyst, obvious SDZ degradation can be clearly observed, and compared with TiO_2-NPs, TiO_2-NSs show higher photoreactivity towards SDZ degradation (Fig. 2A). The degradation curves of SDZ can be well fitted by *pseudo*-first order kinetics equation (Fig. 2B). Here, the photocatalytic degradation rate constant is used to evaluate the photoreactivity of TiO_2 samples (inset of Fig. 2B). It can be seen that the degradation rate constant of SDZ over TiO_2-NSs is 0.035 min^{-1}, which is two time higher than over TiO_2-NPs (rate constant of only 0.17 min^{-1}). As both TiO_2 samples have similar light harvesting ability (Fig. 1B), and the BET surface area of TiO_2-NSs only 63 m^2/g, much smaller than that of TiO_2-NPs (BET surface area of 138 m^2/g), the higher photoreactivity of TiO_2-NSs than that of TiO_2-NPs should be caused by the exposure of reactive high (001) facets instead of by other factors such as light absorption and BET surface area of the photocatalyst.

Further study shows that, after irradiation for 4 h, about 90% of TOC in solution can be removed during the photocatalytic degradation of SDZ (Fig. 2C). In addition, TiO_2-NSs exhibit stable photoreactivity towards SDZ oxidation. Even after 7 successive recycling use, the photoreactivity of SDZ almost keeps unchanged (Fig. 2D), indicating it is promising to be practically used in wastewater treatment.

We also studied the effect of solution pH on the degradation of SDZ degradation in suspensions of TiO_2-NSs, and the results are shown in Fig. S3 (Supporting information). It was found that more than 98% SDZ can be removed in illuminated TiO_2-NSs suspensions in a wide range of solution pH (pH 3.0–11.0) within 120 min. The

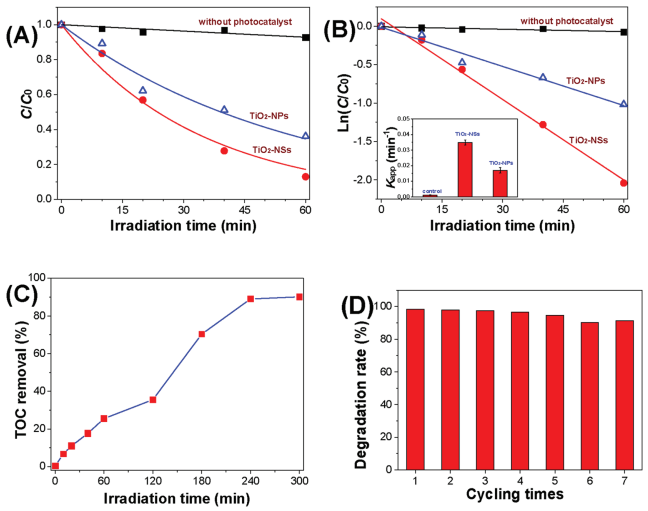

Fig. 2. Photocatalytic degradation profiles of sulfadiazine in the absence and presence of TiO_2 photocatalysts (A) and the corresponding curves fitted by first-order kinetics equation (B), mineralization curve of sulfadiazine in suspensions of TiO_2-NSs as irradiation time (C), and the recycling use of TiO_2-NSs in photocatalytic degradation of sulfadiazine within 120 min (D).

pK_{a1} and pK_{a2} values of SDZ are 1.57 and 6.50, respectively [38]. When the solution pH is greater than 4.16, SDZ exists as a protonated neutral or negatively charged molecule [23], which is easily to be adsorbed on surface of positively charged TiO_2-NSs (zeta potential of 26 mV), facilitating the degradation.

To study the degradation mechanism of SDZ in suspensions of TiO_2-NSs, electron spin resonance (ESR) was used to study the produced reactive oxygen species (ROSs). It was found that obvious signals for DMPO-trapped superoxide radicals ($^{\bullet}O_2^-$) and hydroxyl radicals ($^{\bullet}OH$) were detected (Figs. 3A and B). Both $^{\bullet}O_2^-$ and $^{\bullet}OH$ are typical ROSs, which should be responsible for the efficient degradation and mineralization of SDZ.

We also measured the photocurrent and surface photovoltage spectrum (SPS) of the photocatalyst, which can indirectly reflect the ability of the semiconductor photocatalyst to separate photo-generated charge carriers. From Fig. 3C, it can be clearly seen that the photocurrent of TiO_2-NSs is almost 2 times higher than that of TiO_2-NPs, indicating that the charge carriers of TiO_2-NPs under UV irradiation can be more efficiently separated than that of TiO_2-NPs. Similarly, TiO_2-NSs also exhibits much higher SPS signal than TiO_2-NPs (Fig. 3D). As the photocatalytic activity of TiO_2 is highly related to the number of the separated photo-generated charge carriers, it is not strange to see the superior photoreactivity of TiO_2-NSs compared to TiO_2-NPs (Fig. 2A).

According to the study of Yu *et al.* [39], the co-exposed (101) and (001) facets of high energy TiO_2 nanocrystals can form a surface heterojunction, resulting in the transfer of photo-generated electrons and holes to (101) and (001) facets, respectively. The (101) facets can act as reduction sites, while (001) facets can act as oxidation sites. The spatial separation of charge carriers to

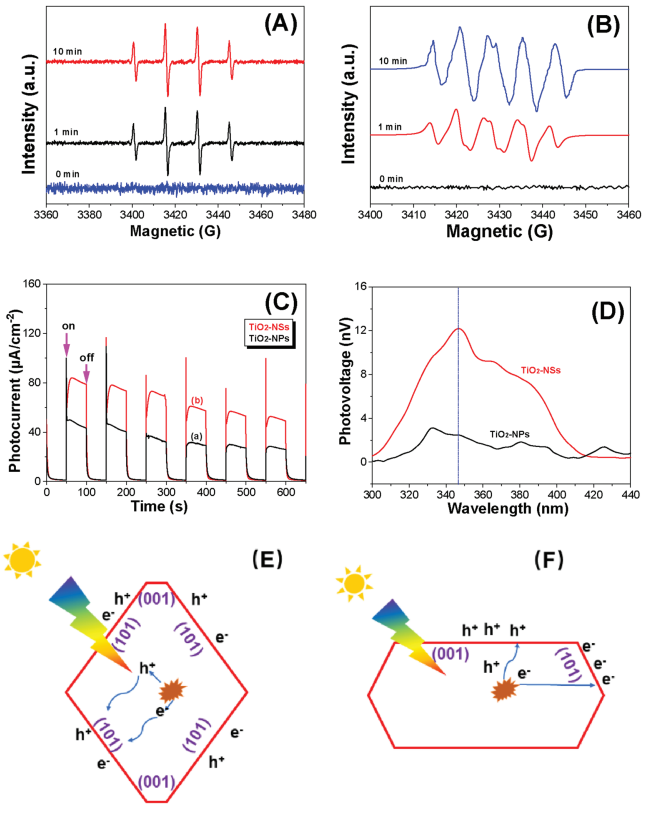

Fig. 3. Time-dependent DMPO spin-trapping ESR spectra for DMPO–$^{\bullet}OH$ in aqueous solution (A) and DMPO–$^{\bullet}OOH/^{\bullet}O_2^-$ (B) in methanol solutions of TiO_2-NSs under the irradiation of UV LED lamp, comparison of the photocurrents (C) and surface photovoltage spectra (D) between TiO_2-NPs and TiO_2-NSs, and migration of photo-generated carriers from the bulk to surface of the photocatalysts between TiO_2-NPs (E) and TiO_2-NSs (F).

different facets can retard the recombination, significantly enhances the photocatalytic activity of TiO_2-NSs. However, as for TiO_2-NPs, most of the photo-generated electrons and holes have to accumulate on the (101) facets due to the smaller percentages of the exposed (001) facets (usually smaller than 5%), which results in an easily recombine, causing a relative lower photoreactivity. In addition, the thickness of TiO_2-NSs is much smaller than that of TiO_2-NPs, which can greatly reduce the charge migration distance from the bulk to the surface of the photocatalyst, facilitating the separation of electrons and holes. Therefore, when compared with TiO_2-NPs (Fig. 3E), TiO_2-NSs (Fig. 3F) exhibits enhanced photoreactivity towards SDZ degradation.

The electrons can be captured by surface adsorbed oxygen to produce $^{\bullet}O_2^-$ radicals, and holes can oxidize solvent water to produce $^{\bullet}OH$ radicals. Under the attacks of $^{\bullet}O_2^-$ and $^{\bullet}OH$ radicals, SDZ steady decomposed and finally mineralized into CO_2 and H_2O.

The 3D fluorescence spectra of the samples obtained with different treatments are showed in Fig. 4. It can be seen from Figs. 4A and B that the fluorescence intensity of SDZ in region I and II (Ex < 250 nm, Em <350 nm) gradually decreased after irradiation for 20 min, suggesting the degradation of SDZ [40]. After photocatalytic oxidation for 60 min, the peaks in region III (Ex < 250 nm, Em > 350 nm) and region V appeared (Fig. 4C), which are commonly correlated with soluble byproducts [41]. After further extending the photocatalytic reaction time for 120 min, obviously enlarged peak area in regions IV (Ex > 250 nm, Em < 380 nm) can be observed, together with the increased fluorescence intensity (Fig. 4D), reflecting the steady formation of degradation intermediates. Thus, the degradation of SDZ might begin from the benzene ring (decreased areas in region I and II), and the following oxidation results in the formation of soluble intermediates (located at regions IV and V).

To reveal the mechanism of SDZ photocatalytic degradation, we analyzed the photodegradation intermediates by LC–MS/MS and screened by MZmine. The detailed data and proposed structures of the intermediates, together with the MS/MS fragments, are shown in Table S1 and Figs. S5–S11 (Supporting information).

On the basis of the elucidated structures of the produced intermediates, transfomation pathways for SDZ degradation in suspensions of TiO_2-NSs under UV light irradiation were proposed in Fig. 5. Briefly, four reaction processes, including hydroxylation, desulfonation, oxidation and cleavage (mainly S-N and C-S) of SDZ, take place during the photocatalytic oxidation process. Since hydroxide radical attacks occurred at sulfonamide group [42,43], benzene ring moiety [44], several hydroxy- and amino-intermediates were identified, such as mono/di-hydroxylated products, as well as suspects Sp1-Sp4. The products cleaved at S-N and C-S sites, including 2-aminopyrimidine, aniline and other intermediates, were also identified.

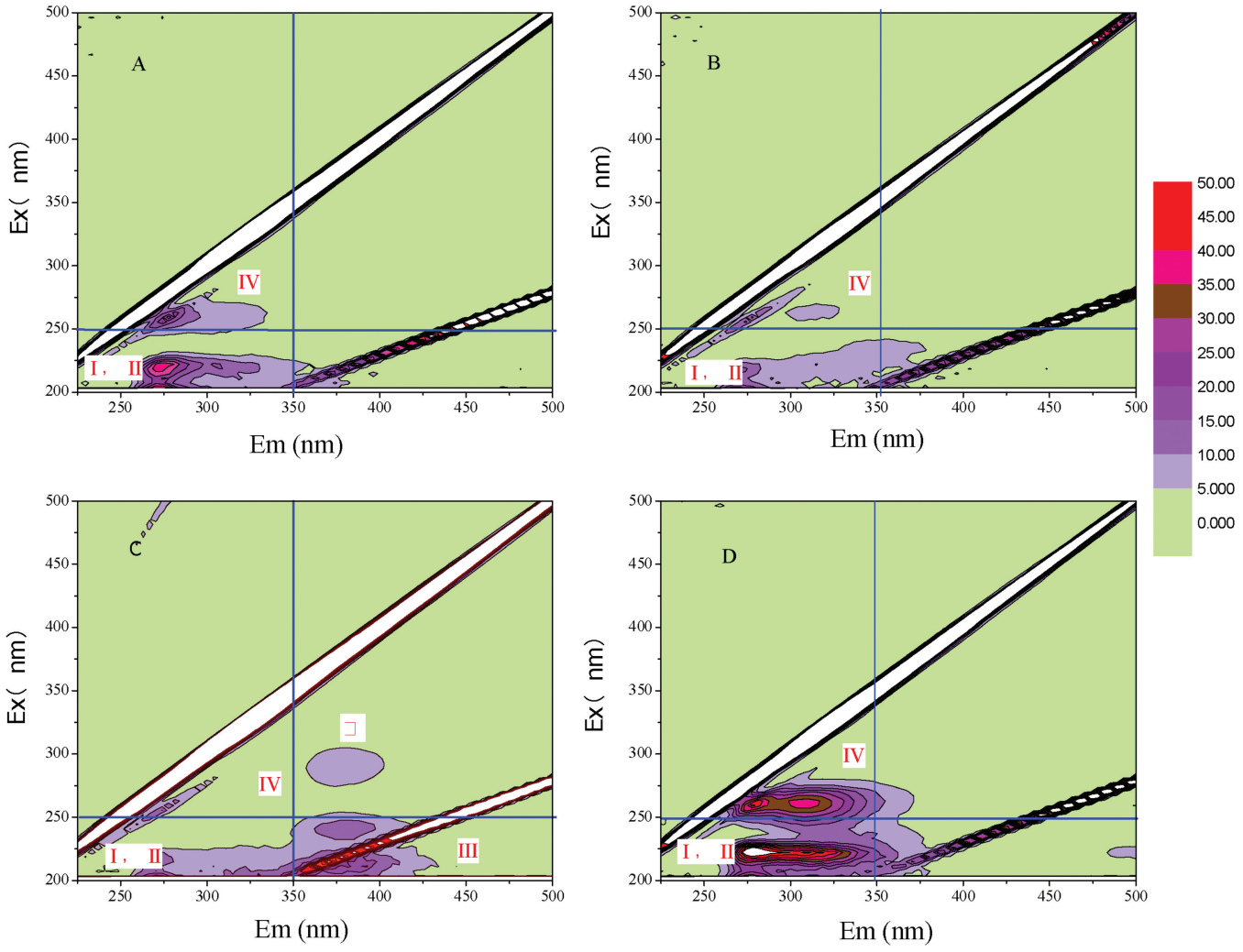

Fig. 4. Time dependent 3D fluorescence spectra of SDZ before (A) and after irradiation for 20 min (B), 60 min (C) and 120 min (D), respectively.

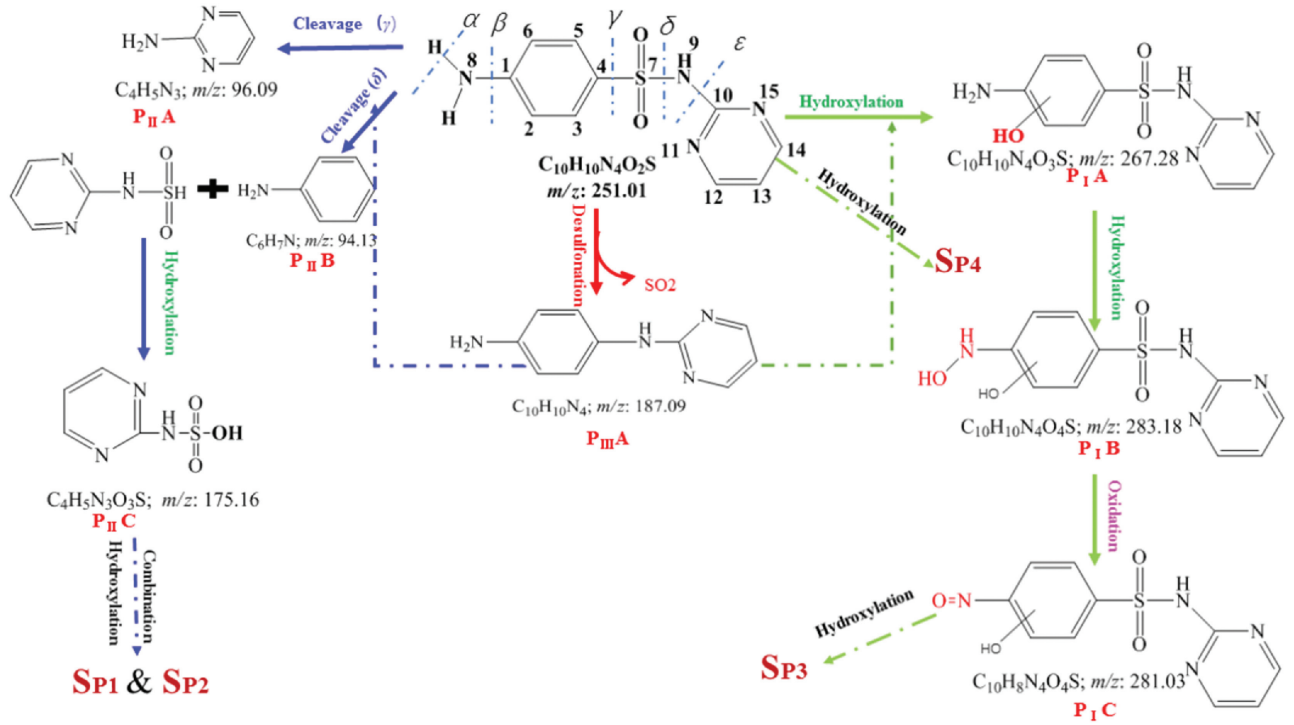

Fig. 5. Possible degradation pathways of sulfadiazine in illuminated TiO_2-NSs suspensions.

Electrophilic attacks of the C2, C6 or N8 atoms on the aromatic ring by $^{\bullet}OH$ radicals lead to the generation of mono-hydroxylated product **P_IA** (Fig. S5) and di-hydroxylated product **P_IB** (Fig. S6) with a molecular weight of 16 Da and 32 Da, respectively, which is higher than that of the parent SDZ (Fig. S5, *m/z* 251.01). Consecutively, these hydrophilic hydroxylated products was further attacked by ROSs such as h^+, $^{\bullet}O_2^-$ and $^{\bullet}OH$, yielding **P_IC** (Fig. S7), including the H- abstraction reaction due to the attack of $^{\bullet}OH$ radicals on N8 amino group. This pathway is considered as a vital photocatalytic reaction for SDZ degradation in UV-irradiated TiO_2 [45].

Bond cleavage was another classic photodegradation pathway of sulfadiazine, which can be cut off directly from β, γ, δ and ε sites [38]. For example, 2-aminopyrimidine (**$P_{II}A$** in Fig. S8) was produced due to the break of δ-site, which has been deemed to commonly occur for sulfonamides degradation [46,47]. The detected aniline (**$P_{II}B$** in Fig. S9) is from the γ-cleavage of SDZ, where S site was further attacked by $^{\bullet}OH$ to form 2-sulfamic acid pyrimidine (**$P_{II}C$** in Fig. S10).

Nucleophilic addition and rearrangement on N9 and C4 of aniline ring occurred to yield **$P_{III}A$** (Fig. S11), proposed as the product generated from the SO_2 extrusion in SDZ molecule [48–50].

Some intermediates that were rarely observed were screened from MZmine peak list by procedure of suspects screening [51]. By simply removal of peaks in blank sample and exclusion of peaks without Lorentzian or Gaussian shape and other procedures, we selected peaks with intensity $>1\times10^7$ (ESI^+) for analysis. Four suspects with 5 peaks were screened (Table S1). The *m/z* 149.0065 (**S_{P4}**) peaks might be double charged ions of trihydroxysulfadiazine. The peaks at *m/z* 353.27 (S_{P1}) and *m/z* 337.3523 (**S_{P2}**) were proposed as a secondary products formed by combination of hydroxylated **$P_{II}C$**. Due to the polyhydroxylated of degradation, a tricharged ion at *m/z* 118.4378 was also observed for **S_{P1}**. The peaks at *m/z* 360.2704 (S_{P3}) was suggested to hexa-hydroxylated **P_IC**. Hence, further studies for the identification of other intermediates are needed in future work.

In summary, compared with TiO_2 nanoparticles, TiO_2 nanosheets exhibit higher photoreactivity towards sulfadiazine degradation. The enhanced photoreactivity of TiO_2 nanosheets is ascribed to the combined effect of (1) shorter migration distance for photo-generated carriers from bulk to the surface of the photocatalyst, (2) exposure of high photo-active (001) facets, and (3) both the exposure of (101) and (001) facets can efficiently retard the recombination of charge carriers, as photo-generated electrons and holes prefer to migrate to (101) and (001) facets due to the different surface energy. Under the attacks of ROSs such as $^{\bullet}O_2^-$ and $^{\bullet}OH$, sulfadiazine steady degraded and mineralized into CO_2 and H_2O. The degradation pathway of sulfadiazine was also proposed by identification of some intermediates through LC–MS/MS techniques. The degradation steps of sulfadiazine include hydroxylation, desulfonation, denitrification, oxidation and cleavage. As TiO_2 nanosheets exhibit relative stability in photocatalytic oxidation of sulfadiazine, the present study developed a potential approach for the remediation of wastewater contaminated by sulfonamides.

Declaration of competing interest

The authors declare that the research was conducted in the absence of any commercial or financial relationships that could be construed as a potential conflict of interest.

Acknowledgments

This study was financially supported by the National Natural Science Foundation of China (Nos. 51672312 and 21976141), the Fundamental Research Funds for the Central Universities: South-Central University for Nationalities (Nos. CZY17016 and CZZ21012),

and Environmental Pollution and Prevention (Team-Construction Project, No. KTZ20043), Undergradate Training Program for Innovation and Entrepreneurship for South-Central University for Nationalities (No. XCX2054).

Appendix A. Supplementary data

Supplementary material related to this article can be found, in the online version, at doi:https://doi.org/10.1016/j.cclet.2021.03.064.

References

[1] K. Kumar, S.C. Gupta, Y. Chander, A.K. Singh, Adv. Agron. 87 (2005) 1–54.
[2] K. Kümmerer, Chemosphere 75 (2009) 417–434.
[3] D. Nematollahi, S.S.H. Davarani, P. Mirahmadpour, et al., Chin. Chem. Lett. 25 (2014) 593–595.
[4] X. Wang, R. Yin, L. Zeng, M. Zhu, Environ. Pollut. 253 (2019) 100–110.
[5] D. Chen, H. Ngo, W. Guo, et al., J. Hazard. Mater. 387 (2020) 121682.
[6] J. Li, Y. Li, Z. Xiong, W. Guo, B. Lai, Chin. Chem. Lett. 30 (2019) 2139–2146.
[7] Q.Q. Zhang, G.G. Ying, C.G. Pan, et al., Environ. Sci. Technol. 49 (2015) 6772–6782.
[8] K.H. Mikkelsen, K.H. Allin, F.K. Knop, Diabetes Obes. Metab. 18 (2016) 444–453.
[9] M.L. Hedgespeth, Y. Sapozhnikov, P. Pennington, A. Clum, et al., Sci. Total Environ. 437 (2012) 1–9.
[10] O. Gonza′lez, C. Sans, S. Espulgas, J. Hazard. Mater. 146 (2007) 459–464.
[11] Y. Deng, Y. Zhang, R. Zhang, et al., Environ. Sci. Technol. 48 (2014) 8212–8218.
[12] D. Xia, H. Liu, B. Xu, et al., Appl. Catal. B: Environ. 245 (2019) 177–189.
[13] D. Xia, Z. Tang, Y. Wang, et al., Chem. Eng. J. 400 (2020) 125894.
[14] C. He, Y. Wang, Z. Li, et al., Environ. Sci. Technol. 54 (2020) 12771–12783.
[15] Y. Huang, M. Luo, S. Li, et al., J. Hazard. Mater. 410 (2021) 124545.
[16] L. Liang, J. Yin, J. Bao, et al., Chin. Chem. Lett. 30 (2019) 167–170.
[17] K. Li, S. Zhang, Y. Li, et al., Chin. J. Catal. 42 (2021) 3–14.
[18] L. Zhang, C. Yang, K. Lv, et al., Chin. J. Catal. 40 (2019) 755–764.
[19] K. Li, M. Zhang, X. Ou, et al., Acta Phys. Chim. Sin. 37 (2021) 2008010.
[20] C. Tan, X. Jian, Y. Dong, et al., Chem. Eng. J. 359 (2019) 594–603.
[21] N. Malesic-Eleftheriadou, E.N. Evgenidou, et al., Chemosphere 234 (2019) 746–755.
[22] A. Zhou, R. Jia, Y. Wang, et al., Sep. Purif. Technol. 234 (2020) 116099.
[23] X. Liu, Y. Liu, S. Lu, et al., Chem. Eng. J. 350 (2018) 131–147.
[24] N. Wang, Y. Yang, Z. Zhou, et al., J. Water Process Eng. 36 (2020) 101335.
[25] Y. Lu, X. Ou, W. Wang, J. Fan, K. Lv, Chin. J. Catal. 41 (2020) 209–218.
[26] G. Huang, X. Liu, S. Shi, et al., Chin. J. Catal. 41 (2020) 50–61.
[27] Z. Hu, K. Li, X. Wu, et al., Appl. Catal. B 256 (2019) 117860.
[28] Z. Hu, X. Li, S. Zhang, et al., Small 16 (2020) 2004583.
[29] Z. Hu, C. Yang, K. Lv, et al., Chem. Commun. 56 (2020) 1745–1748.
[30] D. Gao, R.Y, J. Fan, X. Hong, H. Yu, J. Mater. Sci. Technol. 56 (2020) 122–132.
[31] W. Zhong, X. Wu, Y. Liu, et al., Appl. Catal. B 280 (2021) 119455.
[32] H.G. Yang, S.Z. Qiao, J. Zou, G. Liu, Nature 453 (2008) 638–641.
[33] J.B. Li, X. Wu, S.W. Liu, Acta Phys. Chim. Sin. 37 (2021) 2009038.
[34] Z. Wang, K. Lv, G. Wang, et al., Appl. Catal. B: Environ. 100 (2010) 378–385.
[35] X. Li, X. Wu, S. Liu, et al., Chin. J. Catal. 41 (2020) 1451–1467.
[36] N. Murakami, Y. Kurihara, T. Tsubota, T. Ohno, J. Phys. Chem. C 113 (2009) 3062–3069.
[37] Y. Lu, W. Wang, J. Fan, K. Lv, Chin. J. Catal. 41 (2020) 209–218.
[38] A. Boreen, W.A. Arnold, K. Mcheill, Environ. Sci. Technol. 38 (2004) 3933–3940.
[39] J. Yu, W. Xiao, P. Zhou, M. Jaroniec, J. Am. Chem. Soc. 136 (2014) 8839–8842.
[40] S.R. Ahmad, D.M. Reynolds, Water Res. 33 (1999) 2069–2074.
[41] X.S. He, B.D. Xi, Z.M. Wei, et al., J. Hazard. Mater. 190 (2011) 293–299.
[42] P. Ge, H. Yu, J. Chen, et al., Chemosphere 197 (2018) 569–575.
[43] A.A. Isari, F. Hayati, B. Kakavandi, et al., Chem. Eng. J. 392 (2020) 123685.
[44] S.Y. Mendiola-Alvarez, C. Palomino-Cabello, A. Hernández-Ramírez, et al., J. Photochem. Photobiol. A 394 (2020) 112485.
[45] L. Hu, P.L. Miller, T.J. Strathmann, Water Res. 41 (2007) 2612–2626.
[46] P. Garcia-Munoz, G. Pliego, J.A. Zazo, et al., Chemosphere 180 (2017) 523–530.
[47] D. Song, H. Liu, A. Zhang, J. Qu, RSC Adv. 4 (2014) 48426–48432.
[48] H.L. Tian, H.Q. Fan, J.W. Ma, et al., J. Hazard Mater. 341 (2018) 102–111.
[49] R.M. Baena-Nogueras, E. González-Mazo, P.A. Lara-Martín, Environ. Sci. Technol. 51 (2017) 3148–3156.
[50] M. Feng, J.C. Baum, N. Nesnas, et al., Environ. Sci. Technol. 53 (2019) 2695–2704.
[51] C. Hug, N. Ulrich, T. Schulze, et al., Environ. Pollut. 184 (2014) 25–32.